JOURNAL OF PROPULSION AND POWER
Vol. 23, No. 2, March–April 2007

Effect of Pulse Length and Ejector Radius on Unsteady Ejector Performance

Jack Wilson*
QSS Group, Inc., Cleveland, Ohio 44135

DOI: 10.2514/1.19665

The thrust augmentation of a set of ejectors driven by a shrouded Hartmann–Sprenger tube has been measured at four different frequencies. Each frequency corresponded to a different length to diameter ratio of the pulse of air leaving the driver shroud. Two of the frequencies had length to diameter ratios below the formation number, and two above. The formation number is the value of length to diameter ratio below which the pulse converts to a vortex ring only, and above which the pulse becomes a vortex ring plus a trailing jet. A Box–Behnken statistical design of experiment was performed at each frequency, measuring the thrust augmentation generated by the appropriate ejectors from the set. The parameters were ejector length, radius, and inlet radius. The results showed that there is an optimum ejector radius and length at each frequency. Using a polynomial fit to the data, the results were interpolated to different ejector radii and pulse length to diameter ratios. This showed that a peak in thrust augmentation occurs when the pulse length to diameter ratio equals the formation number, and that the optimum ejector radius is 0.84 times the sum of the vortex ring radius and the core radius.

Nomenclature

A_{pulse} = exit area of the driving jet
a = radius of vortex ring core
D_{pulse} = $2\sqrt{A_{\text{pulse}}/\pi}$ (1.73 in.)
f = frequency of driving jet
K = circulation in vortex ring
L = $\int_o^t u(t)\,\mathrm{d}t$: axial extent of driver pulse at time t
L_{ej} = length of the ejector
L_{pulse} = length of the slug of air in each pulse
$\dot{m}_{\text{jet}}$ = mass flow rate of the jet
m_{pulse} = mass of air in each pulse
$\dot{m}_{\text{total}}$ = total mass flow rate leaving the ejector
N = formation number
p = fraction of total jet momentum in the vortex ring
R = radius of the vortex ring
R_{ej} = radius of the ejector
R_{exit} = exit radius of the ejector
R_s = inner radius of the shroud (1 in.)
r_n = ejector inlet radius
S_t = Strouhal number (fD_{pulse}/U)
T_{ejector} = thrust of jet plus ejector
T_{jet} = thrust of jet alone
t = time
t' = time at which the pulse ratio $L/D_{\text{pulse}} = N$
$u(t)$ = jet velocity as a function of time
U = average velocity of the driving jet $= T_{\text{jet}}/\dot{m}_{\text{jet}}$
V_{exit} = average in time and space of ejector exit velocity
α = thrust augmentation ratio
α_{ss} = thrust augmentation for $L_{\text{pulse}}/D_{\text{pulse}} = \infty$
α_{total} = weighted sum of α_{ss} and α_{vr}
α_{vr} = thrust augmentation due to vortex ring only
$\alpha_{\text{vr}}|_N$ = α_{vr} for $L_{\text{pulse}}/D_{\text{pulse}} = N$
β = mass entertainment coefficient $= (\dot{m}_{\text{total}} - \dot{m}_{\text{jet}})/\dot{m}_{\text{jet}}$
ΔT = thrust measured on ejector alone
ε = a/R
ρ = atmospheric air density
τ = period of one pulse $= 1/f$

Presented as Paper 3829 at the 41st AIAA/ASME/SAE/ASEE Joint Propulsion Conference & Exhibit, Tucson, Arizona, 10–13 July 2005; received 24 August 2005; revision received 24 April 2006; accepted for publication 27 July 2006.

*Senior Engineering Specialist, 21000 Brookpark Road. Associate Fellow AIAA.

I. Introduction

THERE is currently interest in pulsed detonation engines due to their promise of increased efficiency [1–3]. This in turn has revived interest in pulsed ejectors [3–5], because the latter can increase the thrust [2], and potentially reduce the noise level, of such engines with little additional hardware. There have been measurements on pulsed ejector performance in the past, using drivers that were not detonation devices. Lockwood [6], using a pulsejet driver, measured thrust augmentations as high as 1.9, with a very short ejector. Didelle [7], using a jet interrupted by a butterfly valve, also observed a maximum thrust augmentation ratio of 1.9, but with a much longer ejector. Bertin [8], also claimed a thrust augmentation ratio of around 2, but gave few details. More recently, Paxson, Wilson, and Dougherty [9] have repeated Lockwood's experiment, with similar results, although the optimum ejector was rather longer than was Lockwood's. Wilson and Paxson [10], using a Hartmann–Sprenger, or resonance, tube to generate a pulsed jet, measured a maximum thrust augmentation of 1.32, and found, as did Paxson, Wilson, and Dougherty, that there was an optimum radius for the ejector. It was suggested that the optimum ejector size might be related to the size of the vortex ring emerging from the resonance tube. Despite these efforts, it is still not clear what the important parameters are for optimizing a pulsed ejector. Except for that of Didelle, in none of the above experiments was the length of the pulse driving the ejector changed. Didelle, who varied the jet frequency, and hence pulse length, found his maximum thrust augmentation at a Strouhal number of 0.07.

A major feature of any pulsed jet flow is the starting vortex ring (Elder and de Haas [11], Bremhorst and Hollis [12]). Gharib, Rambod, and Shariff [13] have shown that there is a critical value of the pulse length to diameter ratio $L_{\text{pulse}}/D_{\text{pulse}}$, which they called N: for values of $L_{\text{pulse}}/D_{\text{pulse}} < N$, the pulse transforms into a vortex ring only, for $L_{\text{pulse}}/D_{\text{pulse}} > N$, the flow becomes a vortex ring followed by a trailing jet. Moreover, the size of the vortex ring produced increases with $L_{\text{pulse}}/D_{\text{pulse}}$ up to the formation number, but remains fixed above the formation number. Because the structure of the flow changes in this way with $L_{\text{pulse}}/D_{\text{pulse}}$, one would expect that changing $L_{\text{pulse}}/D_{\text{pulse}}$ might also affect ejector performance.

To explore this possibility, it was decided to measure pulsed thrust augmentation using the shrouded Hartmann–Sprenger tube used previously [10], because it gives strong pulses, is simple to operate, and its frequency can be changed. The Hartmann–Sprenger tube, formerly called a resonance tube, was discovered by Hartmann and Trolle [14] in 1922. Originally it consisted of a converging nozzle, producing an underexpanded supersonic jet, blowing into a closed tube situated on the axis of the jet. A shock will form in front of the tube, and if this shock is in a region of shock instability [15], that is, Mach number decreasing with distance, oscillations will occur in which the tube alternately fills with air, swallowing the jet, and then empties while deflecting the jet from the tube [16]. These oscillations can produce intense sound, over 140 db [17], pressure oscillations of 6 atm [16], and temperatures as high as 900 K [18], and, using a vacuum insulated tube, 1000 K [19]. Applications of Hartmann–Sprenger tubes, in addition to being used as sirens, include fog dispersal and ultrasonic drying [17], explosive initiation [15], and proposals for improved mixing for scramjet combustion [20], and as flow control actuators [21]. Brocher [22] has shown that even a correctly expanded jet directed into a tube can oscillate, provided a sting is mounted on the axis of the nozzle. Because there are now no unstable regions, the sensitivity of the tube position is reduced, and high pressures can be generated. Roughly, the pressure at the end of the tube alternates between the external pressure and the stagnation pressure of the driving jet. Thus this version of a Hartmann–Sprenger tube seemed a likely source for a strongly pulsed jet. To create a directed jet, a cylindrical shroud was placed around the nozzle and tube, concentrating the flow into a constant area annular region aligned with the tube axis. Brocher and Pinna [23] have previously used a diverging horn around a Hartmann–Sprenger tube in a similar manner, but their objective was to amplify the acoustic output, and no indication of the velocity field was given. Kastner and Samimy [21] put a shield around the region between nozzle exit and tube entrance, with an opening in it to allow exhaust egress. They imaged the exhaust flow using a sheet laser probe and acetone seeding, and observed wavy structures in the flow. This flow was orthogonal to the axis of the nozzle and tube. Thompson [24] used timed shadowgraphs to observe the flow between the nozzle and the entrance to the tube for an unshielded Hartmann–Sprenger tube, and clearly saw that there are definitely two phases; in the inflow phase, when the jet is filling the tube, there is no external flow, and there is a strong external flow when the tube is emptying. Thus the exhaust flow is indeed a pulsed flow in which the flow cuts off between pulses. Wilson [25] has shown that the shrouded Hartmann–Sprenger tube produces a pulsed flow, consisting of a train of vortices, with the vortices possibly followed by a trailing jet, depending on the value of $L_{\text{pulse}}/D_{\text{pulse}}$.

The frequency of oscillation of a Hartmann–Sprenger tube is approximately the quarter wave frequency based on the tube length [21]. Thus by varying the tube and shroud lengths, different frequencies can be generated, corresponding to different values of the pulse length to diameter ratio. A three level, three parameter Box–Behnken statistical experiment was designed to explore the effects of ejector length, radius, and nose radius. This was repeated at each of four frequencies. The objective was to find optimum ejector designs at each frequency, and see how they were affected by frequency.

II. Apparatus

A photograph of the apparatus is shown in Fig. 1. Consisting of the shrouded Hartmann–Sprenger tube, a thrust plate, and a set of ejectors, it is the same as was used by Wilson and Paxson [10]. The Hartmann–Sprenger tube is shown in Fig. 2, with a Mach 2 axisymmetrical nozzle at the bottom. The nozzle throat has a diameter of 0.5 in., and is aligned with the resonance tube, which was 6 in. long as first built. The nozzle and tube are surrounded by a 2 in. diameter shroud. A needle was aligned with the axis of the nozzle, to stimulate oscillations as described by Brocher [22]. A supply of air at a pressure of 7.8 atm ensured Mach 2 operation exhausting to atmosphere. The average mass was measured upstream of the nozzle, and found to be 0.46 ± 0.002 lb/s, both when pulsing, and at steady

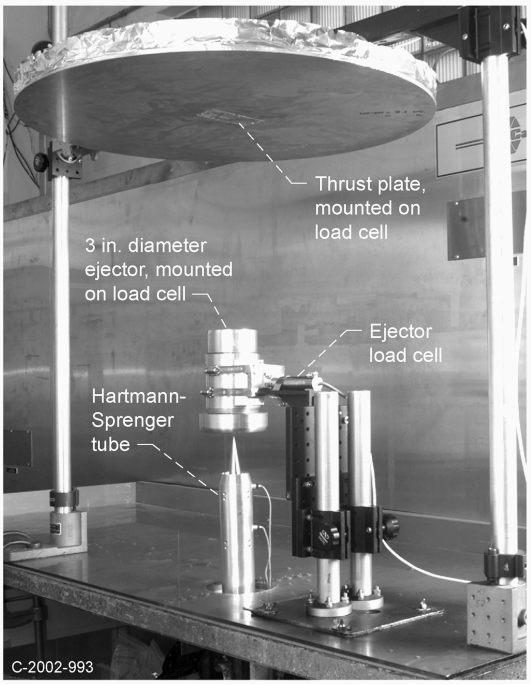

Fig. 1 Photograph of the apparatus.

state without the resonance tube in place. The Hartmann–Sprenger tube is mounted vertically, with the jet flowing upwards. The ejector is mounted above the tube, on a sliding mount so that its height is easily adjustable. Above the ejector is a thrust plate, with a diameter of 30 in., and which constitutes the primary measurement of the thrust of both the jet alone, and the jet plus an ejector. The distance between the thrust plate and the jet exit was set at 26 in. This distance was determined by varying the distance and noting the thrust reading of the jet alone. The apparent thrust increased at first as distance increased, but had leveled off by 26 in. A barrier was placed around the edge of the thrust plate to prevent induced radial flows on the rear of the plate from lowering the pressure behind the plate giving erroneously higher thrust readings [7]. The diameter of the thrust plate must be sufficiently large that the flow on the front leaves the plate in the radial direction [7]. This was verified by putting a wool tuft on the edge of the plate, and observing that it did stand out horizontally when the jet was blowing. The thrust plate is attached to an Omega load cell model LC601-25, having a range of ± 25 lb, to provide an electrical thrust signal. The system was calibrated by adding known weights to the plate, and measuring the response. Similarly, the ejector was attached to another load cell, also a model LC601-25. The signals from each load cell were fed to Agilent model 34401A averaging multimeters. All runs lasted 1 min, during which time the voltmeters stored 180 readings, and then displayed the average value. Each reading lasts 0.167 s, so that at the lowest frequency, a reading is an integration over 20 pulses of the Hartmann–Sprenger tube. At higher frequencies, it is obviously an integration over even more pulses. The experimental procedure involved making three tests to read the thrust of the jet without the ejector, followed by a series of tests with the ejector (two at each setting of jet exit to ejector distance), followed again by three tests reading the thrust of the jet without an ejector. T_{jet}, defined as the average of the six test readings without the ejector, typically measured 10.00 ± 0.11 lb. The thrust augmentation ratio is then given by

$$\alpha = T_{\text{ejector}}/T_{\text{jet}} \tag{1}$$

The signal from the ejector load cell ΔT should correspond to the additional thrust produced by the ejector, that is, $T_{\text{ejector}} - T_{\text{jet}}$. Thus the quantity ϕ, defined as

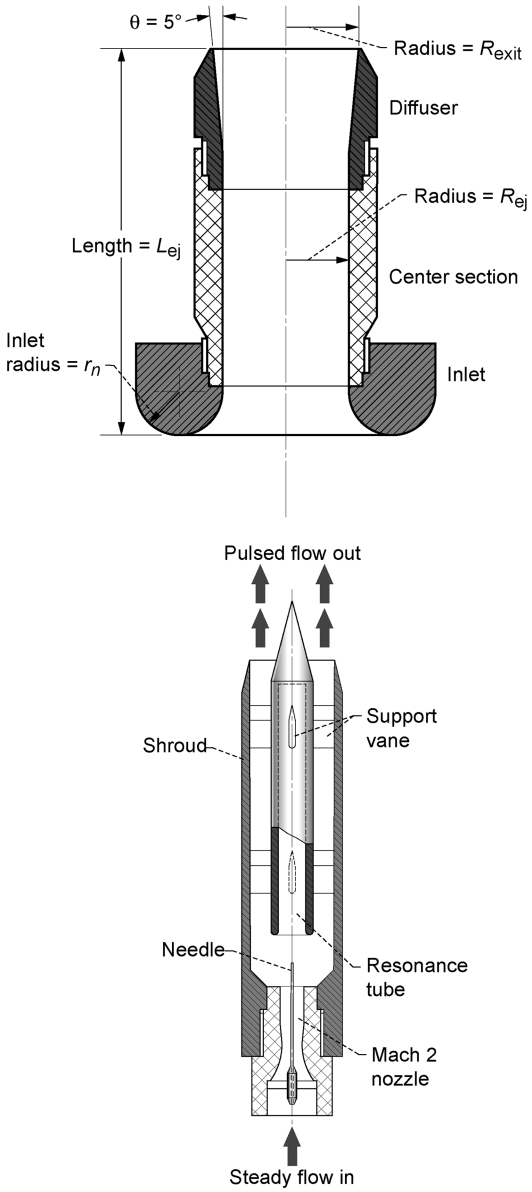

Fig. 2 Schematic diagram of the Hartmann–Sprenger tube and the set of ejectors used in the experiment.

$$\phi = 1 + \Delta T/T_{\text{jet}} \tag{2}$$

should be the same as the thrust plate measurement of α The uncertainty in the measurements of both α and ϕ is ± 0.03. At separation distances between jet exit and ejector entrance close to the maximum thrust augmentation, the two ratios agreed within the uncertainty, and only α will be reported.

In addition to thrust augmentation, it is desirable to measure mass flow entrainment. For this, measurements of the jet mass flow, and the mass flow leaving the ejector are needed. Because the Mach 2 nozzle in the resonance tube is choked, the jet mass flow can be measured upstream of the nozzle, where it will be a steady reading. For this a standard orifice was mounted in the supply line to the jet. The jet flow was measured both as a steady supersonic flow, that is, with the resonance tube removed, and with the resonance tube in place. The resulting mass flow was indeed identical for the two cases, with a value of 0.46 ± 0.002 lb/s.

For measuring the mass flow at the exit of the ejector, the flow was probed with a Thermal Systems, Inc., model IFA 300 hot wire, which provided the radial distribution of velocity at the ejector exit. Measurements of ejector exit velocity were made using the 550 Hz source only, with the $R_{\text{ej}}/R_s = 1.1$ and $R_{\text{ej}}/R_s = 1.5$ ejectors. The signals showed periodic fluctuations in velocity, with the period equal to that of the source. The fluctuations were quite large; for example, with the hot wire on the centerline of the $R_{\text{ej}}/R_s = 1.5$ ejector, the average velocity was 305 ft/s, the maximum was 466 ft/s, and the minimum was 260 ft/s. The hot wire was set at different radial positions, and the velocity measured. The distribution of average velocity as a function of radius is remarkably smooth, and the curves can be integrated to give the volume flow rate, and hence the mass entrainment factor β, defined as ingested mass divided by the jet mass flow. The resulting values of β are 0.9 for the $R_{\text{ej}}/R_s = 1.1$ ejector, and 1.9 for the $R_{\text{ej}}/R_s = 1.5$ ejector. Dividing the volume flow rate by the ejector exit area πR_{exit}^2 gives an average exit velocity, which was 285 ft/s for the $R_{\text{ej}}/R_s = 1.5$ ejector, and 337 ft/s for the $R_{\text{ej}}/R_s = 1.1$ ejector.

Initially, the Hartmann–Sprenger tube operated at a frequency of 550 Hz. Different frequencies were obtained by, first, putting a plug inside the resonance tube to shorten it, which produced a frequency of 1100 Hz, and then making two longer tubes and shrouds to replace the original tube, to give frequencies of 275 and 125 Hz. Because the nozzle upstream of the resonance tube is choked, the mass flow remained the same for all frequencies.

An ejector is also shown in Fig. 2, to illustrate the geometry. To achieve the three parameter, three level, test matrix, a set of ejectors was built, consisting of entrance sections, center sections, and a diffusing tail section. At each ejector radius, three nose sections were made, each having a different nose radius r_n of either 0.25, 0.5, or 0.75 in., plus two center sections of different length, and one tail section. By using either no center section, a short center section, or a long one, three different L_{ej} were obtained, roughly 3, 7.5, and 12 in. Because there was a diffuser on each ejector, the exit radius is greater than the ejector radius itself.

In addition to the ejector length, radius, and inlet radius, thrust augmentation is dependent on the distance between the exit of the driving jet and the entrance to the ejector. This distance was varied for each combination of ejector radius, length, and nose radius, and only the thrust augmentation at the distance giving maximum augmentation for any combination is given in the results.

III. Design of the Experiment

The original experimental design of Wilson and Paxson [10] for a frequency of 550 Hz was chosen to be a statistical design of experiments, three level, three parameter Box–Behnken scheme [26], with L_{ej}/R_s, R_{ej}/R_s, and r_n/R_s as the three parameters. This does not mean to imply that division by R_s is an appropriate scaling; it is simply a convenient way of making the numbers nondimensional. Four values of R_{ej}/R_s were used, namely 1.1, 1.5, 3.0, and 4. It was found that the optimum value of R_{ej}/R_s for thrust augmentation appeared to be shifting up as frequency decreased, so the smallest value of R_{ej}/R_s was omitted for the two lower frequencies, and similarly the highest value of R_{ej}/R_s was omitted for the highest frequency. The full set of runs made is given in Table 1.

IV. Experimental Results

The measurements of thrust augmentation found in the various sets of Box–Behnken runs are given in Table 1 and in Figs. 3a–3d, in which thrust augmentation is plotted against normalized ejector length, L_{ej}/R_s, for each normalized ejector diameter, R_{ej}/R_s, at different values of the normalized nose radius, r_n/R_s. A different gray scale is used for each value of R_{ej}/R_s for both lines and symbols. The 90% confidence level in α is ± 0.03. The data from a Box–Behnken three parameter set can be fitted with a response surface of the form

$$\begin{aligned}\alpha = {} & b_0 + b_1 \cdot (L_{\text{ej}}/R_s) + b_2 \cdot (R_{\text{ej}}/R_s) + b_3 \cdot (r_n/R_s) + b_{11} \\ & \cdot (L_{\text{ej}}/R_s)^2 + b_{22} \cdot (R_{\text{ej}}/R_s)^2 + b_{33} \cdot (r_n/R_s)^2 + b_{12} \cdot (L_{\text{ej}}/R_s) \\ & \cdot (R_{\text{ej}}/R_s) + b_{13} \cdot (L_{\text{ej}}/R_s) \cdot (r_n/R_s) + b_{23} \cdot (R_{\text{ej}}/R_s) \cdot (r_n/R_s)\end{aligned} \tag{3}$$

Table 1 The matrix of test runs comprising the 3 parameter, 3 level statistical experiment at each of the four frequencies used

Run no.	R_{ej}/R_s	L_{ej}/R_s	r_n/R_s	α			
				$f = 1100$	$f = 550$	$f = 275$	$f = 125$
1	1.1	3.125	0.5	1.17	1.155		
2	1.1	7.125	0.25	1.149	1.16		
3	1.1	7.625	0.75	1.134	1.155		
4	1.1	12.375	0.5	1.122	1.092		
5	1.5	2.875	0.25	1.099	1.264		
6	1.5	3.375	0.75	1.053	1.275		
7	1.5	7.375	0.5	1.172	1.330		
8	1.5	7.375	0.5	1.167	1.325		
9	1.5	7.375	0.5	1.169	1.308		
10	1.5	12.125	0.25	1.166	1.255		
11	1.5	12.625	0.75	1.165	1.267		
12	2	3.125	0.5	1.022	1.118		
13	2	7.125	0.25	1.092	1.206		
14	2	7.625	0.75	1.10	1.226		
15	2	12.375	0.5	1.167	1.266		
16	3	3.125	0.5		1.034		
17	3	7.125	0.25		1.075		
18	3	7.625	0.75		1.085		
19	3	12.375	0.5		1.139		
20	1.5	3.125	0.5			1.287	1.14
21	1.5	7.125	0.25			1.320	1.221
22	1.5	7.625	0.75			1.355	1.237
23	1.5	12.375	0.5			1.326	1.265
24	2	2.875	0.25			1.277	1.186
25	2	3.375	0.75			1.343	1.218
26	2	7.375	0.5			1.379	1.317
27	2	7.375	0.5			1.373	1.295
28	2	7.375	0.5			1.376	1.313
29	2	12.125	0.25			1.305	1.271
30	2	12.625	0.75			1.383	1.310
31	3	3.125	0.5			1.053	1.075
32	3	7.125	0.25			1.106	1.137
33	3	7.625	0.75			1.116	1.182
34	3	12.375	0.5			1.197	1.250

where the values of the constants b_{ij} are determined from the data. These were found by inserting the data into a computer program (Seshadri and Demming [27]), which calculates the constants, and values of the confidence level for each constant. The program is essentially a least-squares fit to the data for the three parameters. Because the data were taken at three levels, terms higher than second order cannot be considered. Constants with low confidence level were eliminated, until only terms with levels greater than 90% were retained. The resulting constants are listed in Table 2. Once the response surface is known, the optimum thrust augmentation can be predicted, together with the values of L_{ej}/R_s, R_{ej}/R_s, and r_n/R_s at which the optimum occurs. These values are also listed in Table 2.

Although Eq. (3) includes r_n, changes in α due to changes in r_n for the range of values used are very small, and the changes seen experimentally are statistically insignificant, except at a frequency of 275 Hz where for $R_{ej}/R_s = 2$, thrust for $r_n/R_s = 0.25$ seems lower than values for $r_n/R_s = 0.5$ and $r_n/R_s = 0.75$ indicating an optimum value between the latter two values. That, apart from this one case, changes in the nose radius seem unimportant is surprising, and may be a consequence of the limited values of r_n used in this experiment. Other experiments [9,28] have shown a significant effect of r_n, including the possibility of an optimum value. Sections through the response surface at each value of R_{ej} for $r_n/R_s = 0.5$, are also plotted in Fig. 3, showing good agreement with the experimental results. The optimum predicted values are little different from the maximum observed experimental values. It will be seen that thrust augmentation for $R_{ej}/R_s = 1.1$ is about the same at 1100 Hz and 550 Hz, for $R_{ej}/R_s = 1.5$, and 2, thrust augmentation increases with frequency up to 275 Hz, then decreases for 125 Hz, and for $R_{ej}/R_s = 3$, thrust augmentation continues to increase with frequency. The maximum of thrust augmentation seems to be shifting to higher values of R_{ej}/R_s as the frequency increases.

V. Interpretation of the Experimental Results

A. Statement of the Problem

It was originally hoped that by finding a response surface at each frequency, some insight would be gained into how the parameters affect the thrust augmentation as a function of the frequency. Except for the conclusion that changes in nose radius were not statistically significant, this was not apparent from the constants listed in Table 2. Because the objective here is to find the overall maximum thrust augmentation, and at what values of the parameters this occurs, only the maximum augmentation achieved at any diameter and frequency will be considered further. In other words, it will be assumed that, given an ejector diameter, and the frequency, the optimum length can be determined. This optimum length will be considered further below. A response surface of optimum thrust augmentation will be sought. It was stated above that the nature of the pulsed source changes with the ratio L_{pulse}/D_{pulse}, consisting of a train of vortex rings for $L_{pulse}/D_{pulse} < N$, and a train of vortex rings followed by a trailing jet for $L_{pulse}/D_{pulse} > N$. Also the size of the vortex ring grows with increasing L_{pulse}/D_{pulse} up to $L_{pulse}/D_{pulse} = N$, but remains constant thereafter [13]. It can be expected then that the thrust augmentation might also change depending on whether L_{pulse}/D_{pulse} is greater or less than N. L_{pulse}/D_{pulse} will be taken as one variable for the response surface; its relationship to frequency will be given below. It has been suggested previously [10] that the optimum ejector size may be related to the size of the vortex ring. If so, then as the vortex ring size grows, the optimum ejector size will grow. The vortex ring size can be defined as $R + a$, and the ratio

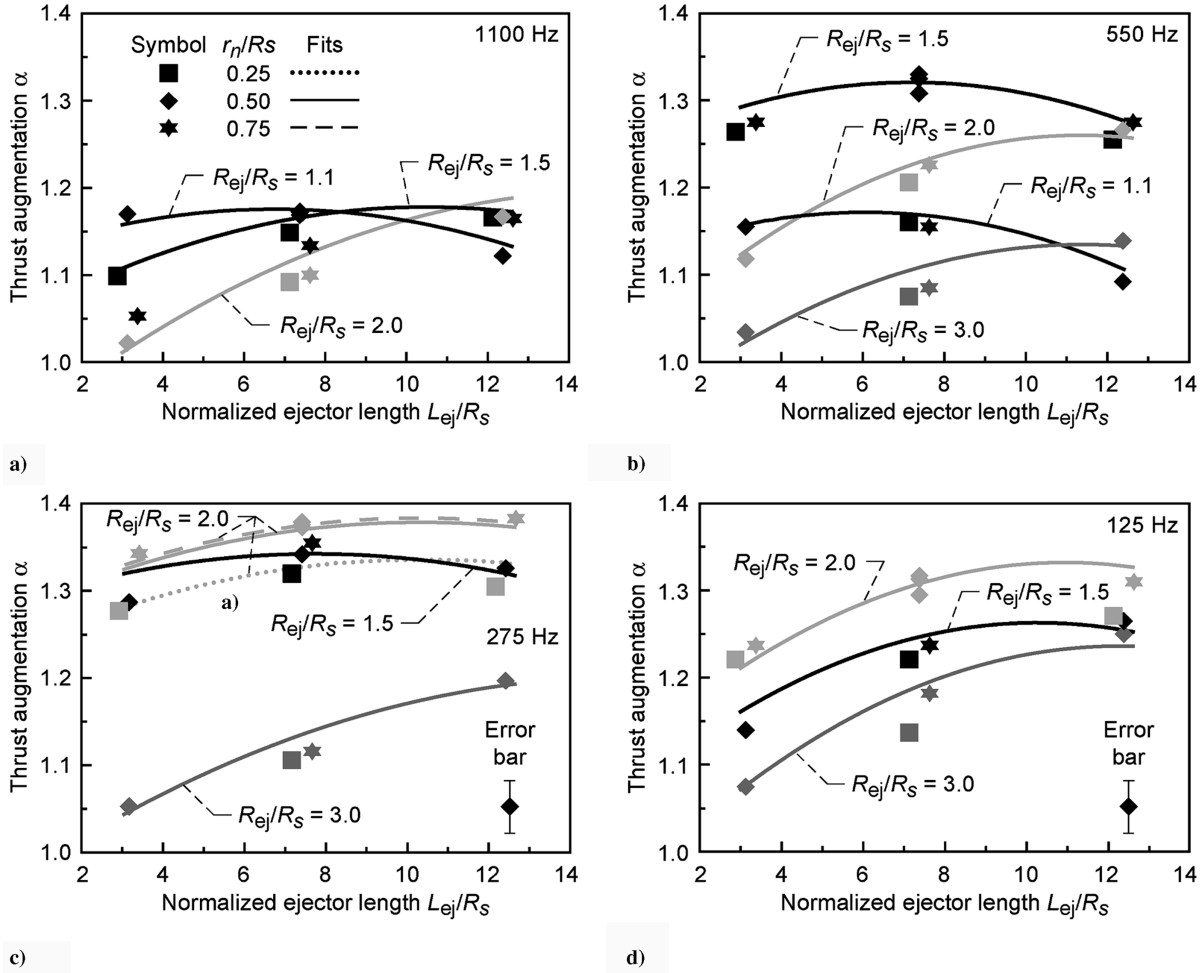

Fig. 3 Results from the statistical experiments at four different frequencies, showing thrust augmentation versus normalized ejector length: a) 1100 Hz; b) 550 Hz; c) 275 Hz; d) 125 Hz. Different symbols are used for each nose radius: ■, $r_n/R_s = 0.25$; ◆, $r_n/R_s = 0.50$; ★, $r_n/R_s = 0.75$. The points are experimental data, the lines are response surface fits: dotted, $r_n/R_s = 0.25$; solid, $r_n/R_s = 0.50$; dashed, $r_n/R_s = 0.75$. A different gray scale is used for each value of R_{ej}/R_s for both lines and symbols.

$(R + a)/R_{ej}$ should be an important parameter, and will be used as the second parameter in the response surface for $L_{pulse}/D_{pulse} < N$. The data that are input for the response surface are given in Table 3. The values of R and a as a function of L_{pulse}/D_{pulse} were derived from slug theory as described by Wilson [25]. Using the slug model plus some experimental measurements Wilson [25] has indicated that the value of the formation number is 6.9 for this shrouded Hartmann–Sprenger tube.

B. Relationship of Frequency to L_{pulse}/D_{pulse}

The experiments were performed at four different frequencies. Because the mass flow was constant at all frequencies, m_{pulse} is given by

$$m_{pulse} = \dot{m}_{jet}/f \tag{4}$$

But m_p is also given by the product of pulse volume and density

$$m_{pulse} = \rho\pi D_{pulse}^2 L_{pulse}/4 \tag{5}$$

Table 2 Constants for Eq. (3): the response surface of the Box–Behnken experimental design, together with predictions for the maximum thrust augmentation at each frequency

	$f = 1100$ Hz	$f = 550$ Hz	$f = 275$ Hz	$f = 125$ Hz
b_0	1.16812	−0.18464	0.54744	0.32863
b_1	−0.01464	−0.00713	——	0.03207
b_2	——	1.81433	0.68699	0.64294
b_3	0.28836	0.23637	0.52521	0.44842
b_{11}	−0.00126	−0.00197	−0.00103	−0.00193
b_{22}	−0.07511	−0.62527	−0.19356	−0.15947
b_{33}	−0.41306	−0.21744	−0.30355	−0.39603
b_{12}	0.02336	0.02591	0.01052	0.00505
b_{13}	0.01187	——	——	
b_{23}	——	——	−0.06310	
α_{max}	1.189	1.331	1.385	1.338
R_{ej}/R_s	1.98	1.62	1.91	2.21
L_{ej}/R_s for α_{max}	12.6	8.9	9.9	11.2
r_n/R_s	0.5	0.5	0.75	0.5
L_{ej}/R_s	6.36	5.49	5.18	5.07

Table 3 L_{pulse}/D_{pulse} for each frequency used, together with the maximum thrust augmentation observed for each R_{ej}/R_s, and values of $(R + a)/R_{ej}$

Frequency (Hz)	1100		550		275		125	
L_{pulse}/D_{pulse}	2.5		5		10		22	
	α_{max}	$(R + a)/R_{ej}$	α_{max}	$(R + a)/R_{ej}$	α_{max}	$(R + a)/R_{ej}$	α_{max}	$(R + a)/R_{ej}$
$R_{ej}/R_s = 1.1$	1.17	1.331	1.16	1.654	——		——	
$R_{ej}/R_s = 1.5$	1.169	0.976	1.321	1.213	1.355	1.343	1.265	1.343
$R_{ej}/R_s = 2$	1.167	0.732	1.266	0.91	1.376	1.007	1.308	1.007
$R_{ej}/R_s = 3.0$	——		1.139	0.607	1.197	0.671	1.25	0.671

Table 4 Values of p as a function of L_{pulse}/D_{pulse} for the jet velocity of the Hartmann–Sprenger tube

L_{pulse}/D_{pulse}	6.86	7.4	8	10	12	14	16	18	20	22	24	∞
$p=$	1	0.9736	0.9424	0.8064	0.6724	0.5742	0.5002	0.4443	0.3990	0.3649	0.3363	0

from which it is seen that, because D_{pulse} is constant, L_{pulse}, and also L_{pulse}/D_{pulse}, is inversely proportional to frequency. In Table 3 the values of L_{pulse}/D_{pulse} for each frequency used are given. The two higher frequencies have values of L_{pulse}/D_{pulse} below the formation number, whereas the two lower frequencies have values of L_{pulse}/D_{pulse} above it.

C. Thrust Augmentation for L_{pulse}/D_{pulse} Greater than N

For the measurements at values of L_{pulse}/D_{pulse} above the formation number, the flow consists of a leading vortex ring and a trailing jet. The vortex ring has exactly the same size and properties as that generated at $L_{pulse}/D_{pulse} = N$. The thrust on the ejector will be partially due to the vortex ring and partially to the trailing jet. There will be a time t' following initiation of the jet at which the value of $L = \int_o^{t'} u(t)^2\,dt$ is equal to $N.D_{pulse}$. The fraction of the total jet impulse that is in this portion of the jet is

$$p = \int_o^{t'} u(t)^2\,dt \Big/ \int_o^{\tau} u(t)^2\,dt \tag{6}$$

It is this fraction of the impulse that goes into forming the vortex ring, giving rise to α_{vr}. The remaining impulse will be in the trailing jet, which is assumed to be quasisteady, and therefore will create the same α_{ss} as would a steady jet. Thus, for L_{pulse}/D_{pulse} greater than the formation number, the total thrust augmentation will be

$$\alpha_{total} = p\alpha_{vr} + (1 - p)\alpha_{ss} \tag{7}$$

in which α_{vr} is calculated at the formation number, that is, it is $\alpha_{vr}|_N$. It should be stated here that Eq. (7) is an assumption. A linear addition of the two terms seems the simplest assumption that could be made, and is certainly correct in the limits of $p = 1$ and $p = 0$, but it is not proved. On the other hand, there does not appear to be any theoretical guidance as to what else to use.

A measurement of $u(t)$ for this tube has been reported previously (Wilson [25]). Given this distribution, the integrals which determine p can be performed numerically. The result is given in Table 4. Of course, if $L_{pulse}/D_{pulse} < N$, then $\alpha_{total} = \alpha_{vr}$, with no contribution from α_{ss}.

At each of the two low frequencies, the value of p is known from Table 4, that is, $p = 0.8064$ at $L_{pulse}/D_{pulse} = 10$, and 0.3649 at $L_{pulse}/D_{pulse} = 22$. At each frequency, there are three values of α_{total}, one for each different ejector radius. Thus for each radius, there are two values of α_{total}, which can be substituted into an Eq. (7) for each frequency, so that the resulting pair of equations can be solved for $\alpha_{vr}|_N$, and α_{ss}. Values of $\alpha_{vr}|_N$, and α_{ss} are given in Table 5.

The values of α_{ss} for each ejector radius are fitted by the equation

$$\alpha_{ss} = 1.094 + 0.158\,\ell n(2R_{exit}/D_{pulse}) \tag{8}$$

in which the variable $2R_{exit}/D_{pulse}$ was used as steady-state thrust augmentation has been shown to correlate with the ratio of ejector exit area to jet area ratio [30]. As can be seen, α_{ss} increases as the ratio of ejector exit diameter to tube diameter increases. This trend, and the values of the thrust augmentation are in agreement with values of steady-state thrust augmentation given by Porter and Squyers [30]. Fancher [29] has predicted that the maximum steady-state thrust augmentation ratio for $2R_{exit}/D_{pulse}$ between 2.24 and 3.74 is given approximately by

$$\alpha_{ss} = 1.075 + 0.025(2R_{exit}/D_{pulse})^2 \tag{9}$$

Values of α_{ss} derived from this equation are listed in Table 5, and are not very different from the values of α_{ss} found in this study.

Table 5 Values of $\alpha_{vr}|_N$ and α_{ss} derived from the data for L_{pulse}/D_{pulse} above N, together with values of α_{ss} from Fancher [29]

R_{ej}/R_s	1.5	2.0	3.0
$\alpha_{vr}|_N$	1.395	1.406	1.174
α_{ss}, Eq. (8)	1.191	1.252	1.294
α_{ss}, Eq. (9)	1.15	1.208	1.375

D. Thrust Augmentation for L_{pulse}/D_{pulse} less than N

The objective of this work is to gain some understanding of the conditions which lead to maximum thrust augmentation, in particular ejector radius, and vortex ring size. Length is, of course, also an important parameter, but the value of $L_{ejector}/R_{ejector}$ at α_{max}, also given in Table 2, and plotted in Fig. 4, can be considered as a dependent variable, that is, given a value of L_{pulse}/D_{pulse}, the optimum value of $L_{ejector}/R_{ejector}$ can be selected from Fig. 4, and then the length determined for any given ejector diameter. At $L_{pulse}/D_{pulse} = N$, the value of $L_{ejector}/R_{ejector}$ for α_{max} is 5.2–5.5.

To investigate the effects of ejector radius and vortex ring size, the values of maximum thrust augmentation observed at the two higher frequencies, together with the values calculated for $\alpha_{vr}|_N$ from the low frequency data, were used as values of the dependent parameter

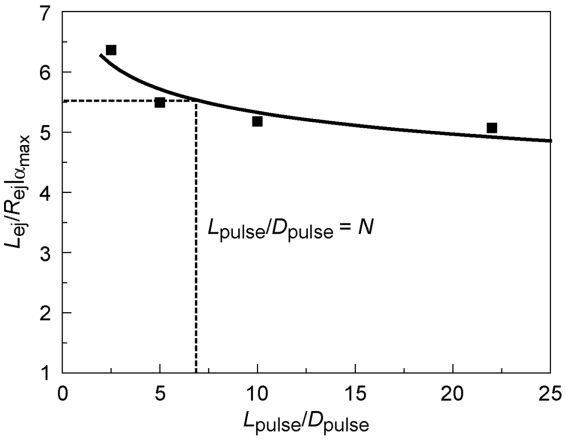

Fig. 4 L_{ej}/R_{ej} at α_{max} versus L_{pulse}/D_{pulse}.

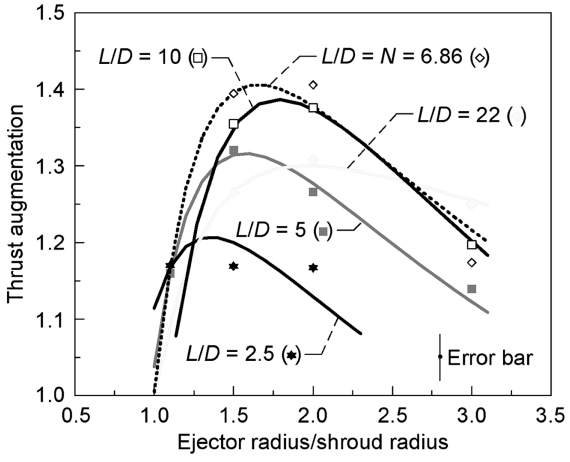

Fig. 5 Thrust augmentation versus R_{ej}/R_s. The data and fitted lines correspond to different values of $L_{\text{pulse}}/D_{\text{pulse}}$, namely: $L_{\text{pulse}}/D_{\text{pulse}} = 2.5$, black solid line, ★; $L_{\text{pulse}}/D_{\text{pulse}} = 5$, dark gray solid line, ■; $L_{\text{pulse}}/D_{\text{pulse}} = N$, dotted line, ◇; $L_{\text{pulse}}/D_{\text{pulse}} = 10$, thick black solid line, □; $L_{\text{pulse}}/D_{\text{pulse}} = 22$, light gray solid line, ◆.

in creating a response surface in parameter space, with $L_{\text{pulse}}/D_{\text{pulse}} = N$ and $(R + a)/R_{\text{ej}}$ as the two independent parameters.

The values of thrust augmentation given in Table 3 ($\alpha_{\max}$) and Table 5 ($\alpha_{\text{vr}}|_N$) were entered into a nonlinear regression analysis, with the resulting fit being:

$$\alpha = 1.105 - 0.6358[(R + a)/R_{\text{ej}} - 1.005]^2 + 0.039[(R + a)/R_{\text{ej}}]L_{\text{pulse}}/D_{\text{pulse}} \tag{10}$$

Using this fit, together with thrust augmentation calculated from Eq. (7) for $L_{\text{pulse}}/D_{\text{pulse}}$ greater than N, thrust augmentation is plotted against ejector radius in Fig. 5, and against $L_{\text{pulse}}/D_{\text{pulse}}$ in Fig. 6. In Fig. 6, the short horizontal lines at the right represent the values of α_{ss} for $R_{\text{ej}}/R_s = 1.5$, 2, and 3. From the second term of Eq. (10) it is clear that there is an optimum value of R_{ej} which is indeed close to $(R + a)$.

VI. Discussion

The plot of thrust augmentation versus ejector radius in Fig. 5 shows that the optimum ejector radius increases as $L_{\text{pulse}}/D_{\text{pulse}}$ increases, as had already been observed from Fig. 2. The optimum

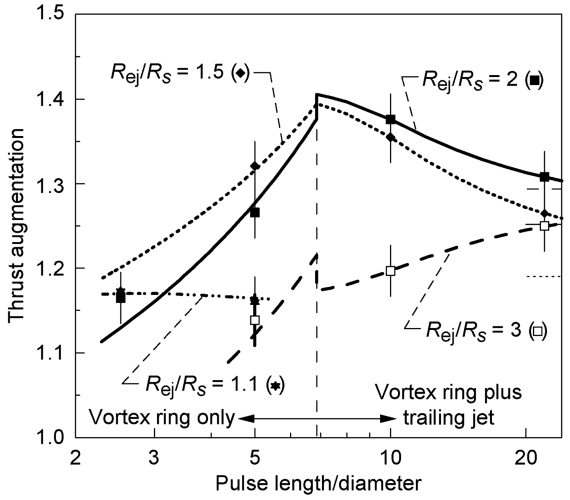

Fig. 6 Thrust augmentation versus $L_{\text{pulse}}/D_{\text{pulse}}$ for each value of R_{ej}/R_s. The horizontal lines at the right represent the values of α_{ss}. The data and fitted lines correspond to different values of R_{ej}/R_s, namely: $R_{ej}/R_s = 1.1$, dash–dotted line, ★; $R_{ej}/R_s = 1.5$, dotted line, ◆; $R_{ej}/R_s = 2$, solid line, ■; $R_{ej}/R_s = 3$, dashed line, □.

ejector radius for $L_{\text{pulse}}/D_{\text{pulse}} = N$ is at $R_{\text{ej}}/R_s = 1.7$, which corresponds to $R_{\text{ej}}/(R + a) = 0.84$, that is, the optimum ejector is slightly smaller than the vortex ring size. The plot of thrust augmentation against $L_{\text{pulse}}/D_{\text{pulse}}$ in Fig. 6 shows that there is a peak thrust augmentation at $L_{\text{pulse}}/D_{\text{pulse}} = N$. However, as $L_{\text{pulse}}/D_{\text{pulse}}$ gets very much larger than N, the thrust augmentation approaches α_{ss}, which increases monotonically with R_{exit}, and so there will no longer be an optimum ejector radius at very large $L_{\text{pulse}}/D_{\text{pulse}}$. The optimum thrust augmentation at $L_{\text{pulse}}/D_{\text{pulse}} = N$ is around 1.4, considerably lower than the values around 2.0 reported by Lockwood [6], Didelle [7], Paxson, Wilson, and Dougherty [9]. It has been shown (Wilson [25]) that the circulation produced by the annular exit of the shrouded Hartmann–Sprenger tube ($K = 13.7$ m^2/s) is lower than would be expected for the same value of U from a circular exit ($K = 20$ m^2/s). Because the vortex ring velocity is proportional to the circulation, a circular exit would have a higher value of vortex ring velocity, and hence, presumably, also a higher value of V_{exit}. If it is also assumed that the thrust augmentation is proportional to V_{exit}/U, then a circular tube producing the same exit velocity as the Hartmann–Sprenger tube could be expected to generate a thrust augmentation of 2.04, in line with the values from the other experiments.

These experiments indicate that a length of about two and a half times the ejector diameter is optimum. This is longer than claimed by Lockwood [6], but shorter than optimum length to diameter ratios found by Paxson, Wilson, and Dougherty [9], or Didelle [7], The results given in Table 2 for the optimum ejector length to diameter ratio seem to show a gradual decrease in the ratio as $L_{\text{pulse}}/D_{\text{pulse}}$ increases. Thus the discrepancy in optimum ejector length to diameter between this work and those of Lockwood, Paxson, Wilson, and Dougherty might be explained as due to being in very different regimes of $L_{\text{pulse}}/D_{\text{pulse}}$. Didelle's maximum thrust augmentation was at a Strouhal number of 0.07. Because his valve gave two pulses per second, the value of $L_{\text{pulse}}/D_{\text{pulse}}$ used by Didelle is $1/2S_t$, that is, 7 at maximum thrust augmentation. Most of his runs were for $L_{\text{pulse}}/D_{\text{pulse}} < 7$, with a few at $L_{\text{pulse}}/D_{\text{pulse}} = 10$. It is gratifying that Didelle's optimum value of $L_{\text{pulse}}/D_{\text{pulse}}$ is in close agreement with that found here, but that leaves the discrepancy of the optimum ejector length to diameter ratio unexplained.

In these experiments, Didelle's experiments, and the experiments with pulsejet drivers, the length of the pulse increases with the inverse of the frequency, and so low frequency approaches steady-state flow. Both Didelle [7], and Wilson and Paxson [10], found that V_{exit} had a large average component, with an oscillation on top of it, such that the ejector flow never reached zero velocity. Care must be used in relating the results to pulse detonation devices, where the pulse length is determined by the length of the tube, and is independent of frequency. Because the duty cycle is very low in detonation devices, V_{exit} may drop to zero between pulses. This is less likely as the frequency increases, and so high frequency is more likely to approach a steady-state flow in the ejector.

VII. Conclusions

In conclusion, for the jet produced by the shrouded Hartmann–Sprenger tube, unsteady thrust augmentation is shown to have a peak when the driving jet pulse has a pulse length to diameter ratio equal to the formation number. For values of $L_{\text{pulse}}/D_{\text{pulse}}$ close to N, the optimum ejector radius will be equal to $0.84\,(R + a)$. As $L_{\text{pulse}}/D_{\text{pulse}}$ increases, the optimum ejector radius also increases, until for very large values of $L_{\text{pulse}}/D_{\text{pulse}}$, the thrust augmentation approaches steady-state values, increasing monotonically with ejector radius. The optimum ejector length appears to be about 2.5 times the ejector diameter.

Acknowledgments

The author wishes to thank Robert Pastel and Kevin Dougherty for assistance with the experiments. The support of the CVCCE project, directed by Leo Burkardt, is acknowledged with gratitude.

References

[1] Heiser, W. H., and Pratt, D. T., "Thermodynamic Cycle Analysis of Pulse Detonation Engines," *Journal of Propulsion and Power*, Vol. 18, No. 1, 2002, pp. 68–76.

[2] Kentfield, J. A. C., "Fundamentals of Idealized Air-Breathing Pulse-Detonation Engines," *Journal of Propulsion and Power*, Vol. 18, No. 1, 2002, pp. 77–83.

[3] Shehadeh, R., Saretto, S., Lee, S.-Y., Pal, S., and Santoro, R. J., "Thrust Augmentation Experiments for a Pulse Detonation Driven Ejector," AIAA Paper AIAA-2004-3398, July 2004.

[4] Allgood, D. E., Gutmark, E., Hoke, J., Bradley, R., and Schauer, F., "Performance Measurements of Pulse Detonation Engine Ejectors," AIAA Paper 2005-223, Jan. 2005.

[5] Rasheed, A., Tangirala, V., Pinard, P. F., and Dean, A. J., "Experimental and Numerical Investigations of Ejectors for PDE Applications," AIAA Paper 2003-4971, July 2003.

[6] Lockwood, R. M., "Interim Summary Report on Investigation of the Process of Energy Transfer from an Intermittent Jet to Secondary Fluid in an Ejector-Type Thrust Augmenter," Hiller Aircraft Rept. No. ARD-286, 1961.

[7] Didelle, H., "L'Augmentation de Poussée des Trompes à Jets Pulsants ou Battants," Doctor of Engineering Thesis, Scientific and Medical University and the National Polytechnical Institute, Grenoble, France, 1976.

[8] Bertin, J., "Dilution Pulsatoire sur Réacteur," *Comptes Rendus de Séances de l'Académie des Sciences*, Vol. 240, May 1955, pp. 1855–1857.

[9] Paxson, D. E., Wilson, J., and Dougherty, K. T., "Unsteady Ejector Performance: An Experimental Investigation Using a Pulsejet Driver," AIAA Paper 2002-3915, July 2002.

[10] Wilson, J., and Paxson, D. E., "Unsteady Ejector Performance: An Experimental Investigation Using a Resonance Tube Driver," AIAA Paper 2002-3632, July 2002.

[11] Elder, F. K., and de Haas, N., "Experimental Study of the Formation of a Vortex Ring at the Open End of a Cylindrical Shock Tube," *Journal of Applied Physics*, Vol. 23, No. 10, 1952, pp. 1065–1069.

[12] Bremhorst, K., and Hollis, P. G., "Velocity Field of an Axisymmetric Pulsed, Subsonic Air Jet," *AIAA Journal*, Vol. 28, No. 12, 1990.

[13] Gharib, M., Rambod, E., and Shariff, K., "A Universal Time Scale for Vortex Ring Formation," *Journal of Fluid Mechanics*, Vol. 360, April 1998, pp. 121–140.

[14] Hartmann, J., and Trolle, B., "On a New Method for the Generation of Sound Waves," *Physical Review*, Vol. 20, No. 6, 1922, pp. 719–727.

[15] Marchese, V. P., Rakowsky, E. L., and Bement, L. J., "A Fluidic Sounding Rocket Motor Ignition System," *Journal of Spacecraft and Rockets*, Vol. 10, No. 11, 1973, pp. 731–734.

[16] Brocher, E., Maresca, C., and Bournay, M.-H., "Fluid Dynamics of the Resonance Tube," *Journal of Fluid Mechanics*," Vol. 43, Pt. 2, Aug. 1970, pp. 369–384.

[17] Brun, E., and Boucher, R. M. G., "Research on the Acoustic Air-Jet Generator: A New Development," *Journal of the Acoustical Society of America*, Vol. 29, No. 5, 1957, pp. 573–583.

[18] Sarohia, V., and Back, L. H., "Experimental Investigation of Flow and Heating in a Resonance Tube," *Journal of Fluid Mechanics*, Vol. 94, Pt. 4, Oct. 1979, pp. 649–672.

[19] Ackeret, J., "The Role of Entropy in the Aerospace Sciences," *Journal of the Aerospace Sciences*, Vol. 28, No. 2, 1961, pp. 81–102.

[20] Bogdanoff, D. W., "Advanced Injection and Mixing Techniques for Scramjet Combustors," *Journal of Propulsion and Power*, Vol. 10, No. 2, 1994, pp. 183–190.

[21] Kastner, J., and Samimy, M., "Development and Characterization of Hartmann Tube Fluidic Actuators for High-Speed Flow Control," *AIAA Journal*, Vol. 40, No. 10, 2002, pp. 1926–1934.

[22] Brocher, E., "Contribution à l'Étude des Générateurs Acoustique à Jet d'Air," *Acustica*, Vol. 32, No. 4, 1975, pp. 227–235.

[23] Brocher, E., and Pinna, G., "Aeroacoustical Phenomena in a Horn Excited by a Hartmann–Sprenger Tube," *Acustica*, Vol. 45, No. 3, 1980, pp. 180–189.

[24] Thompson, P. A., "Jet-Driven Resonance Tube," *AIAA Journal*, Vol. 2, No. 7, 1964, pp. 1230–1233.

[25] Wilson, J., Wernet, M. P., and Paxson, D. E., "Vortex Rings Generated by a Shrouded Hartmann–Sprenger Tube," *AIAA Journal* (to be published); AIAA Paper 2005-5163, June 2005.

[26] Mason, R. L., Gunst, R. F., and Hess, J. L., *Statistical Design and Analysis of Experiments: With Applications to Engineering and Science*, Wiley, New York, 1989.

[27] Seshadri, S., and Demming, S. N., "Box-B Interactive Computer Programs for Using Three- and Four-Factor Box–Behnken Designs in Research, Development, and Manufacturing (Ver. 2.1)," Statistical Programs, 9941 Rowlett, Suite 6, Houston, TX 77075.

[28] Wilson, J., Sgondea, A., Paxson, D. E., and Rosenthal, B. N., "Parametric Investigation of Thrust Augmentation by Ejectors on a Pulsed Detonation Tube," AIAA Paper 2005-4208, July 2005; *Journal of Propulsion and Power* (submitted for publication).

[29] Fancher, R. B., "Low-Area Ratio, Thrust-Augmenting Ejectors," *Journal of Aircraft*, Vol. 9, No. 3, March 1972.

[30] Porter, J. L., and Squyers, R. A., "A Summary/Overview of Ejector Augmentor Theory and Performance, Phase 2," Technical Rept., Vought Corporation Advanced Technology Center Rept. No. R-91100/9CR-47A, 1979.

J. Powers
Associate Editor